ACS Photonics

pubs.acs.org/journal/apchd5

Article

Low Dark Current High Gain InAs Quantum Dot Avalanche Photodiodes Monolithically Grown on Si

Baile Chen,*,∇ Yating Wan,∇ Zhiyang Xie, Jian Huang, Ningtao Zhang, Chen Shang, Justin Norman, Qiang Li, Yeyu Tong, Kei May Lau, Arthur C. Gossard, and John E. Bowers

Cite This: *ACS Photonics* 2020, 7, 528−533

Read Online

ACCESS | Metrics & More | Article Recommendations

ABSTRACT: Avalanche photodiodes (APDs) on Si operating at optical communication wavelength band are crucial for the Si-based transceiver application. In this paper, we report the first O-band InAs quantum dot (QD) waveguide APDs monolithically grown on Si with a low dark current of 0.1 nA at unit gain and a responsivity of 0.234 A/W at 1.310 μm at unit gain (−5 V). In the linear gain mode, the APDs have a maximum gain of 198 and show a clear eye diagram up to 8 Gbit/s. These QD-based APDs enjoy the benefit of sharing the same epitaxial layers and processing flow as QD lasers, which could potentially facilitate the integration with laser sources on a Si platform.

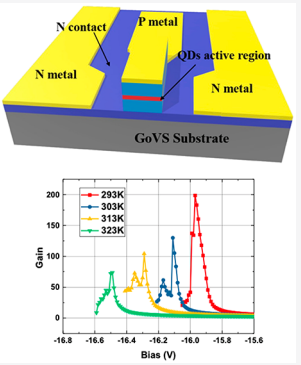

KEYWORDS: *quantum dots, silicon, avalanche photodiodes, gain, bandwidth*

Self-assembled quantum dot (QD) semiconductor nanostructures have attracted intense interest for optoelectronics devices applications due to their unique three-dimensional carrier confinement characteristics. Recently, O-band InAs QD lasers monolithically grown on Si substrate have been demonstrated with low threshold current, high temperature stability, and record-long device lifetime, which could potentially overcome the lack of a laser source in Si photonics.[1−4] Meanwhile, high performance optical amplifiers,[5] near-infrared PIN waveguide photodiodes (PDs),[6,7] and midwavelength infrared QD photodetectors[8−10] with similar QD structures on Si have been recently reported. The three-dimensional carrier confinement in the QDs leads to ultralow dark current density of 3.5×10^{-7}A/cm^2 in QD PDs directly grown on (001) Si, together with a decent responsivity of around 0.2 A/W in the O-band.[6]

Avalanche photodiodes (APDs) can achieve a high internal current gain by applying a high reverse bias voltage due to the avalanche effect, which can significantly improve the signal-to-noise ratio.[11] Driven by the increasing applications in optical communications, monolithic Si−Ge APDs have been demonstrated with large gain-bandwidth products.[12] Recently, InAs QD APDs heterogeneously integrated on Si have been reported with a low dark current of 0.01 nA and a high gain bandwidth product of 240 GHz.[13] In this work, we use an alternative approach through direct epitaxy for better economy of scale and better integration with QD lasers and demonstrate the first InAs QD APDs monolithically grown on (001) Si with a low dark current of 0.1 nA in a 3×50 μm^2 device biased at −5 V. The corresponding dark current density is as low as 6.7×10^{-5} A/cm^2, which is among the best reported values for any III−V PDs grown on a Si substrate at the same reverse bias.[14−17] In addition, the PDs achieve a decent responsivity of 0.234 A/W at 1310 nm at unit gain, limited by coupling into the photodetector waveguide. The dark current at 99% of breakdown voltage is 1.3 nA, and an avalanche gain of up to 198 has been demonstrated. Due to RC and carrier trapping limits, the APDs show a 3 dB bandwidth of 2.26 GHz at −6 V. Temperature studies have been carried out to understand the physics of the avalanche process in the devices. The limiting factors of the current device have been analyzed, and future improvements are discussed. When the high gain and low dark current performance up to 323 K (50 °C) are considered, these APDs hold great potential for applications in energy-efficient interconnects within supercomputers and data centers.

DEVICE STRUCTURE AND FABRICATION

The structure of the photodiode is shown in Figure 1. The QD APD structure was grown on a GaAs-on-V-grooved-Si (GoVS)

Received: December 4, 2019
Published: January 8, 2020

https://dx.doi.org/10.1021/acsphotonics.9b01709
ACS Photonics 2020, 7, 528−533

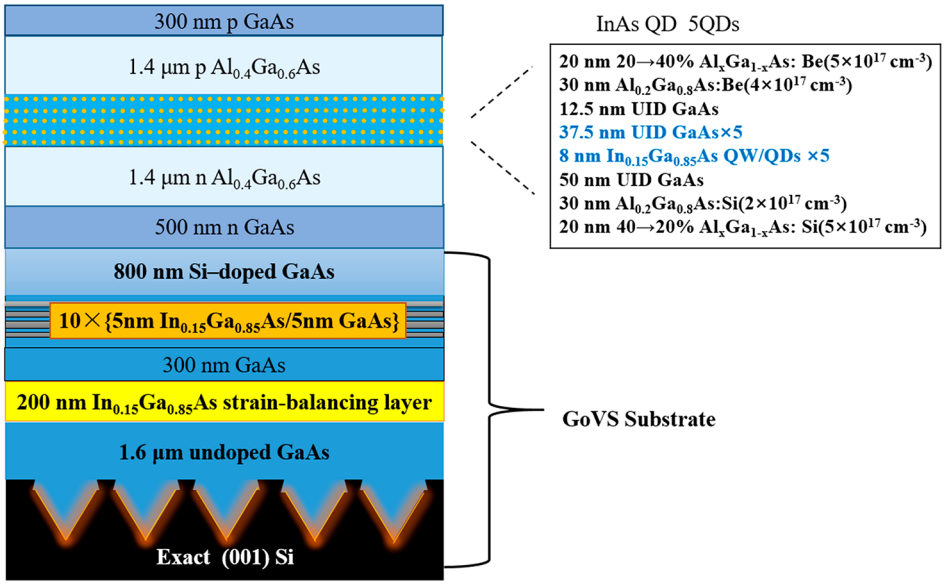

Figure 1. Schematic diagram of the InAs QD APD grown on GoVS substrate.

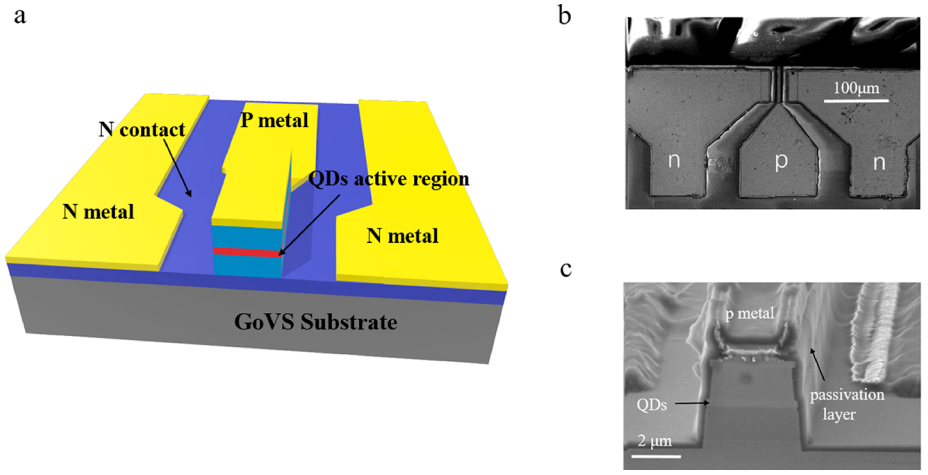

Figure 2. (a) Schematic diagram of the fabricated waveguide photodetector. (b) Top-view and (c) cross-sectional view of the fabricated device.

substrate, prepared by aspect ratio trapping (ART) in a metal–organic chemical vapor deposition (MOCVD) system.[18,19] The APD epitaxial structure was grown in a molecular beam epitaxy (MBE) system. The active region of the PD consists of five-stacked InAs dot-in-a-well (DWELL) structures with a dot density of 6×10^{10} cm^{-2}.

After the material growth, the epitaxial structure was processed into waveguide-shape APD devices with mesa widths ranging from 3 to 50 μm and mesa lengths of 50 μm by inductive coupled plasma (ICP) etching. After ICP etching, the sidewall was passivated with a 12 nm atomic-layer deposited (ALD) Al_2O_3 together with a 1 μm-thick SiO_2 layer to help suppress the surface leakage current. Pd/Ti/Pd/Au and Pd/Ge/Pd/Au were evaporated as metal contact stacks with a 150 μm pitch-size standard ground-signal-ground (GSG) pad. Finally, facets were cleaved with no additional antireflection coatings. The full device structure is schematically shown in Figure 2a. Top-view and cross-sectional view scanning electron microscope (SEM) images of a fabricated device are shown in Figure 2b,c, respectively.

MEASUREMENT AND ANALYSIS

The dark current voltage ($I-V$) curves of a 3×50 μm^2 APD device were measured from 260 to 340 K in a low temperature probe station and recorded by a semiconductor device analyzer (Keysight 1500) as shown in Figure 3a. The device shows a very low dark current of 0.1 nA at 300 K under a bias voltage of −5 V, which corresponds to a low dark current density of 6.6×10^{-5} A/cm^2. This can be attributed to the high crystal quality and surface passivation of the PD mesa. Moreover, the dark current at 300 K was measured to be 1.3 nA around −15.9 V, which is around 99% of the breakdown voltage (−16 V). It is also noted that the breakdown voltage of the APD increases as the temperature increases, which indicates the dominance of avalanche breakdown over tunneling in the APD structure. The capacitance voltage ($C-V$) characteristics of several different sizes of APD devices were also measured at room temperature as shown in Figure 3b; a parasitic capacitance of 517 fF was extracted on the basis of the device area−capacitance curve in the inset of Figure 3b.

The gain versus bias voltage of the device at various temperatures was measured as shown in Figure 4a with an

https://dx.doi.org/10.1021/acsphotonics.9b01709
ACS Photonics 2020, 7, 528−533

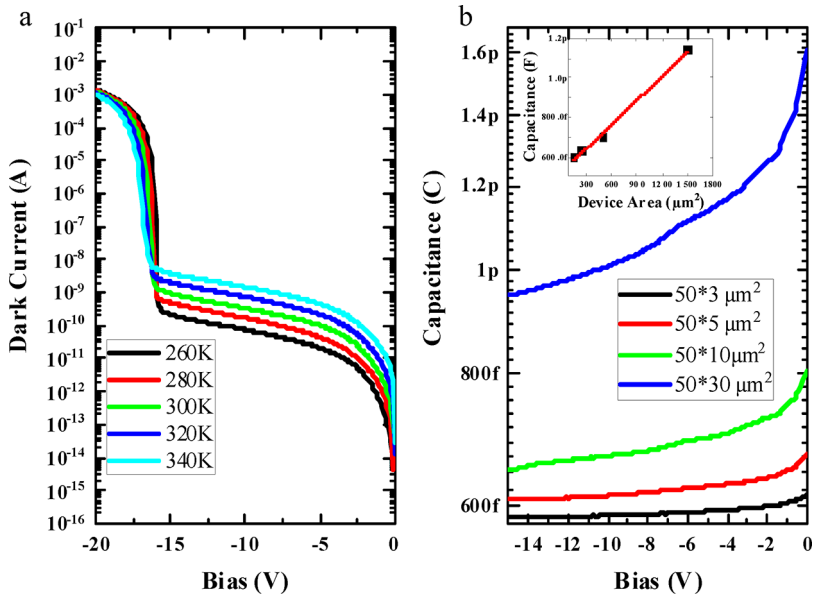

Figure 3. (a) Temperature dependent measurement of the current−voltage characteristics of a 3 × 50 μm^2 device. (b) Capacitance voltage characteristics of devices with different sizes at room temperature. Inset: measured capacitance of a series of devices under −5 V bias.

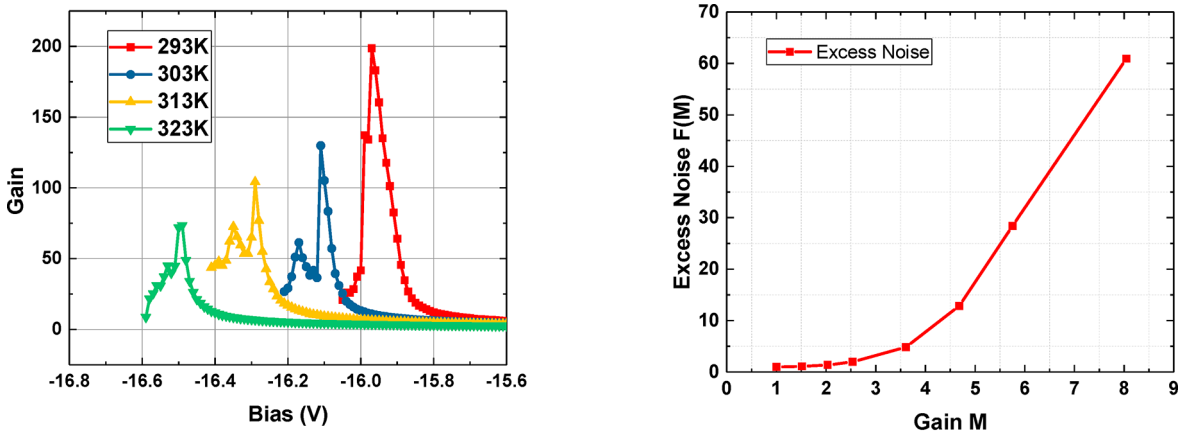

Figure 4. (a) APD gain versus the reverse bias at various temperatures. (b) Excess noise of the APD versus the gain.

input wavelength of 1300 nm. Here, we take the unity gain bias of −5 V to make sure the device is fully depleted. The maximum gain value of 198 was obtained at 293 K (20 °C) and drops to around 73 at 323 K (50 °C). It is also noted that the dark current of the APD is only 33 nA while a maximum gain value of 198 is achieved at a reverse bias of −15.97 V at 293 K (20 °C). This dark current value is more than 2 orders of magnitude lower than that of Si/Ge APDs,[20] InGaAs/InAlAs APDs on Si,[15] and the recent InAs QD APDs heterogeneously integrated on Si.[13] The excess noise of the APD is also measured by a noise figure meter as shown in the Figure 4b. The excess noise is high due to the mixed injection in the APD device, and further optimization for minimizing the noise performance is necessary for future work.

Optical response of the APD was measured by coupling light with a lensed fiber from an O-band tunable laser source to the cleaved facet of the PDs and adjusting the input polarization by a polarization controller. Figure 5a shows wavelength dependence of responsivity for a 3 × 50 μm^2 device at different biases. The input power was fixed at −20 dBm so that the APD is not

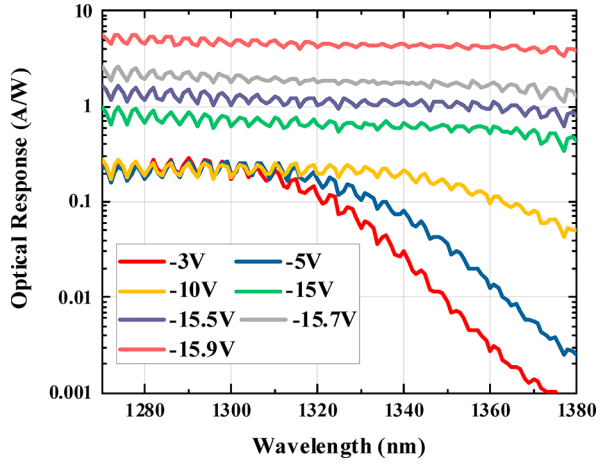

Figure 5. Wavelength dependence of APD responsivity at various biases.

https://dx.doi.org/10.1021/acsphotonics.9b01709
ACS Photonics 2020, 7, 528−533

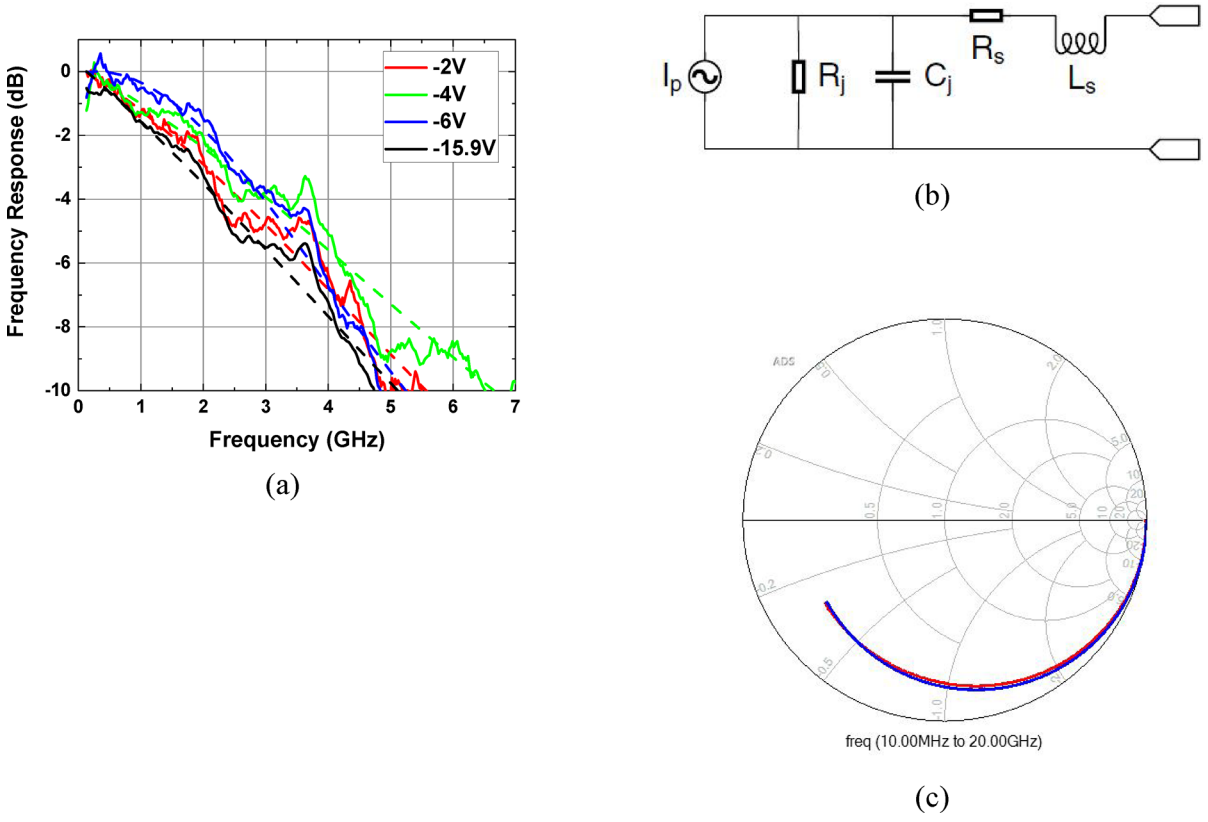

Figure 6. (a) Small-signal frequency responses of the 3.0 × 50 μm^2 device for various bias voltages. (b) Equivalent circuit model used for the fitting of the impedance measurement. (c) Measured (red) and fitted (blue) curves of reflection S_{11} characteristics from 10 MHz to 20 GHz at −6 V.

saturated during the measurement at a high gain condition. The coupling loss between the spherical-lensed fiber and the cleaved facet was estimated to be roughly 3 dB, which is estimated by comparing the measured power from an integrated sphere power meter and a fiber coupled power meter of a forward biased laser diode with the same epilayer structure and the same mesa width of the PD in this work. The oscillatory features shown in the responsivity plot are due to the Fabry−Perot resonance between the rear and the front facets, which has also shown up in other waveguide PD structures.[7] The responsivity of the device at −5 V is 0.234 A/W at 1310 nm and cuts off around 1360 nm, which corresponds to the bandgap of the InAs QD materials. The corresponding absorption coefficient at 1310 nm is estimated to be 770 cm^{-1}, assuming a confinement factor of 6.5%. As the reverse bias increases, the cutoff wavelength red shifts due to the quantum-confined Stark effect (QCSE), which shifts the electron states to lower energies and the hole states to higher energies, respectively, in the QD layers. At a reverse bias of 15.9 V, the responsivity of the APD around 1310 nm increased to 4.8 A/W, due to the avalanche gain of around 20 in the APD structure.

The small-signal frequency response S_{21} was measured using a lightwave-component analyzer (LCA) with a 1310 nm internal light source. The modulated light from LCA was input to the PD facet through a lensed fiber. *Frequency response characteristics* (S_{21}) of a 3 × 50 μm^2 device biased at various voltages are presented in Figure 6a. As shown in Figure 6a, the 3 dB bandwidth increases slightly as the reverse bias increases from −2 to −6 V, which is due to the reduction of both carrier transport time and carrier emission time out of the quantum dots as the electrical field in the absorption region increases. The 3 dB bandwidth of the device is 2.26 and 2.06 GHz at the biases of −6 and −15.9 V, respectively. The bandwidth reduction at −15.9 V is due to the avalanche buildup time. To assess the bandwidth limiting factors, S_{11} characteristics were measured and the parameters were fitted with an equivalent circuit model (Figure 6b), as shown in Figure 6c.[21,22] The circuit parameters were de-embedded from the S_{11} characteristics, giving rise to a calculated RC limited bandwidth of 5.16 GHz with the corresponding fitting parameters shown in Table 1. This RC limited bandwidth is slightly larger than the measured bandwidth value; it is expected that the device performance may be limited by both RC and transit time. As one of the future works, the semi-insulator Si substrate or thick benzocyclobutene (BCB) layer or SU8 layer can be used for material growth and device fabrication to minimize the parasitic capacitance in the device, which could potentially improve the RC limited performance.[23,24]

Table 1. Fitting Parameters in the Circuit Model Figure 6b

R_s (Ω)	R_j (MΩ)	C_j (fF)	L_s (fH)	$f_{RC3\ dB}$ (GHz)
9.38	800	520	1.08e-9	5.16

Figure 7 shows the eye diagram of a 3.0 × 50 μm^2 avalanche photodiode biased at −15.9 V and operating at a 2.5, 5, and 8 Gbit/s data rate. $2^{31}-1$ pseudorandom binary sequences (PRBSs) were generated as the data source to drive an O-band lithium-niobate (LN) modulator, which modulates the 1.31 μm optical signal coming from an external tunable laser. The modulated light signal was controlled to be TE light by a polarization controller and was used as an input to the device

https://dx.doi.org/10.1021/acsphotonics.9b01709
ACS Photonics 2020, 7, 528−533

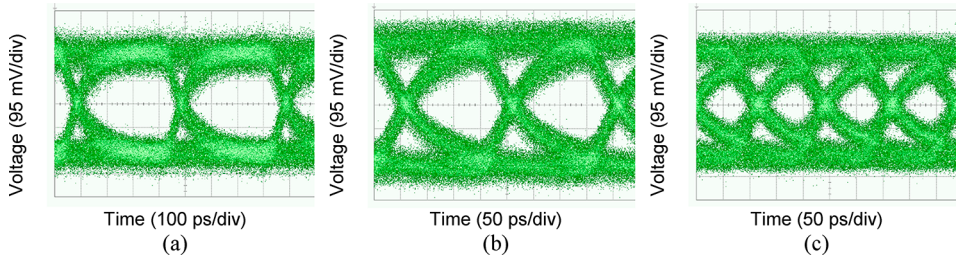

Figure 7. Measured eye diagrams at a bias voltage of −15.9 V for data rates of 2.5, 5, and 8 Gbit/s.

through a spherical lensed fiber with an output−input power of ∼−3 dBm. Clear eye opening up to a data rate of 8 Gbit/s is demonstrated, which indicates that these APDs can be used in an O-band optical communications system. The bit error rate (BER) test at different bias points was conducted using an Anritsu Bit Error Rate Tester at 2.5 Gb/s at room temperature, as shown Figure 8. Photodiodes operated at high gain bias point of −15.9 V exhibit a significantly improved bit error rate as compared to the lower bias point with the same input optical power.

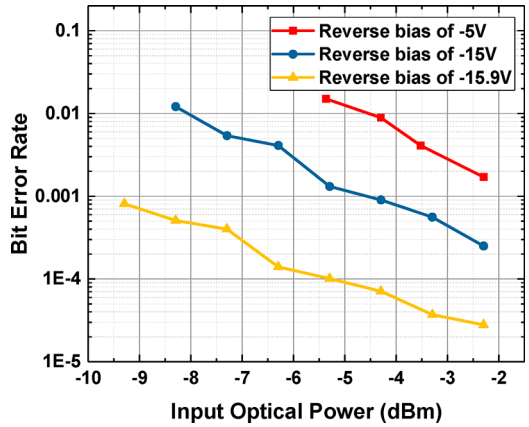

Figure 8. BER versus input optical power of a 3 μm × 50 μm PD with different reverse bias points at 1310 nm.

It is also noted that the APD structure demonstrated in this work is based on the PIN QD structures operated under high reverse bias. The QD layer here acts as both an absorption region and a multiplication region, which could cause a high excess noise in the APD considering the mixed carrier injection.[11] The expected high excess noise of the APD also limited the signal-to-noise ratio when operated at a high gain bias point. One way to overcome this drawback is to incorporate the separated absorption, charge, and multiplication avalanche photodiode (SACM-APD) for low noise and high speed applications.[25,26]

CONCLUSIONS

In summary, we reported the first InAs QD APDs grown on (001) Si using the same epitaxial layers and fabrication process for a QD laser. A low dark current density of 6.7×10^{-5}A/cm^2 has been achieved, which is more than 2 orders of magnitude lower than Ge/Si APDs. A high avalanche gain up to 198 was demonstrated, and the limiting factors of the 3 dB bandwidth of these QD APDs have been investigated. Open eye diagrams were measured up to 8 Gbit/s, which show potential for the O-band optical communications system.

AUTHOR INFORMATION

Corresponding Author

Baile Chen − *University of California Santa Barbara, Santa Barbara, California, and ShanghaiTech University, Shanghai, China;* orcid.org/0000-0002-3265-5787; Email: chenbl@shanghaitech.edu.cn

Other Authors

Yating Wan − *University of California Santa Barbara, Santa Barbara, California;* orcid.org/0000-0003-2157-2406

Zhiyang Xie − *ShanghaiTech University, Shanghai, China*

Jian Huang − *ShanghaiTech University, Shanghai, China;* orcid.org/0000-0002-8728-0505

Ningtao Zhang − *ShanghaiTech University, Shanghai, China*

Chen Shang − *University of California Santa Barbara, Santa Barbara, California*

Justin Norman − *University of California Santa Barbara, Santa Barbara, California*

Qiang Li − *Hong Kong University of Science and Technology, Kowloon, Hong Kong*

Yeyu Tong − *University of California Santa Barbara, Santa Barbara, California, and The Chinese University of Hong Kong, Sha Tin, Hong Kong*

Kei May Lau − *Hong Kong University of Science and Technology, Kowloon, Hong Kong*

Arthur C. Gossard − *University of California Santa Barbara, Santa Barbara, California*

John E. Bowers − *University of California Santa Barbara, Santa Barbara, California*

Complete contact information is available at: https://pubs.acs.org/10.1021/acsphotonics.9b01709

Author Contributions

$^{\nabla}$B.C. and Y.W. contributed equally to this work.

Notes

The authors declare no competing financial interest.

ACKNOWLEDGMENTS

This work was funded in part by the National Key Research and Development Program of China (2018YFB2201000, 2019YFB2203400), in part by the Shanghai Sailing Program (17YF1429300), in part by ShanghaiTech University startup funding (F-0203-16-002), and in part by the Advanced Research Projects Agency-Energy (ARPA-E), U.S. Department of Energy, under Award Number DE-AR0001042.

https://dx.doi.org/10.1021/acsphotonics.9b01709
ACS Photonics 2020, 7, 528−533

REFERENCES

(1) Chen, S.; Liao, M.; Tang, M.; Wu, J.; Martin, M.; Baron, T.; Seeds, A.; Liu, H. Electrically pumped continuous-wave 1.3 μm InAs/GaAs quantum dot lasers monolithically grown on on-axis Si (001) substrates. *Opt. Express* **2017**, *25* (5), 4632−4639.

(2) Chen, S.; Li, W.; Wu, J.; Jiang, Q.; Tang, M.; Shutts, S.; Elliott, S. N.; Sobiesierski, A.; Seeds, A. J.; Ross, I.; et al. Electrically pumped continuous-wave III−V quantum dot lasers on silicon. *Nat. Photonics* **2016**, *10* (5), 307.

(3) Wan, Y.; Zhang, S.; Norman, J. C.; Kennedy, M.; He, W.; Liu, S.; Xiang, C.; Shang, C.; He, J.-J.; Gossard, A. C.; et al. Tunable quantum dot lasers grown directly on silicon. *Optica* **2019**, *6* (11), 1394−1400.

(4) Norman, J. C.; Jung, D.; Wan, Y.; Bowers, J. E. Perspective: The future of quantum dot photonic integrated circuits. *APL Photonics* **2018**, *3* (3), No. 030901.

(5) Liu, S.; Norman, J.; Dumont, M.; Jung, D.; Torres, A.; Gossard, A. C.; Bowers, J. E.; Liu, S.; Torres, A.; Gossard, A.; et al. High-Performance O-Band Quantum-Dot Semiconductor Optical Amplifiers Directly Grown on a CMOS Compatible Silicon Substrate. *ACS Photonics* **2019**, *6* (10), 2523−2529.

(6) Huang, J.; Wan, Y.; Jung, D.; Norman, J.; Shang, C.; Li, Q.; Lau, K. M.; Gossard, A. C.; Bowers, J. E.; Chen, B. Defect Characterization of InAs/InGaAs Quantum Dot p-i-n Photodetector Grown on GaAs-on-V-Grooved-Si Substrate. *ACS Photonics* **2019**, *6* (5), 1100−1105.

(7) Wan, Y.; Zhang, Z.; Chao, R.; Norman, J.; Jung, D.; Shang, C.; Li, Q.; Kennedy, M.; Liang, D.; Zhang, C.; et al. Monolithically integrated InAs/InGaAs quantum dot photodetectors on silicon substrates. *Opt. Express* **2017**, *25* (22), 27715−27723.

(8) Chen, W.; Deng, Z.; Guo, D.; Chen, Y.; Mazur, Y.; Maidaniuk, Y.; Benamara, M.; Salamo, G. J.; Liu, H.; Wu, J.; et al. Demonstration of InAs/InGaAs/GaAs Quantum Dots-in-a-well Mid-wave Infrared Photodetectors Grown on Silicon Substrate. *J. Lightwave Technol.* **2018**, *36* (13), 2572−2581.

(9) Huang, J.; Guo, D.; Deng, Z.; Chen, W.; Liu, H.; Wu, J.; Chen, B. Midwave Infrared Quantum Dot Quantum Cascade Photodetector Monolithically Grown on Silicon Substrate. *J. Lightwave Technol.* **2018**, *36* (18), 4033−4038.

(10) Wu, J.; Jiang, Q.; Chen, S.; Tang, M.; Mazur, Y. I.; Maidaniuk, Y.; Benamara, M.; Semtsiv, M. P.; Masselink, W. T.; Sablon, K. A.; et al. Monolithically integrated InAs/GaAs quantum dot mid-infrared photodetectors on silicon substrates. *ACS Photonics* **2016**, *3* (5), 749−753.

(11) Campbell, J. C. Recent Advances in Avalanche Photodiodes. *J. Lightwave Technol.* **2016**, *34* (2), 278−285.

(12) Kang, Y.; Liu, H.-D.; Morse, M.; Paniccia, M. J.; Zadka, M.; Litski, S.; Sarid, G.; Pauchard, A.; Kuo, Y.-H.; Chen, H.-W.; et al. Monolithic germanium/silicon avalanche photodiodes with 340 GHz gain−bandwidth product. *Nat. Photonics* **2009**, *3* (1), 59.

(13) Tossoun, B.; Kurczveil, G.; Zhang, C.; Descos, A.; Huang, Z.; Beling, A.; Campbell, J. C.; Liang, D.; Beausoleil, R. G. Indium arsenide quantum dot waveguide photodiodes heterogeneously integrated on silicon. *Optica* **2019**, *6* (10), 1277−1281.

(14) Geng, Y.; Feng, S.; Poon, A. W.; Lau, K. M. High-speed InGaAs photodetectors by selective-area MOCVD toward optoelectronic integrated circuits. *IEEE J. Sel. Top. Quantum Electron.* **2014**, *20* (6), 36−42.

(15) Yuan, Y.; Jung, D.; Sun, K.; Zheng, J.; Jones, A. H.; Bowers, J. E.; Campbell, J. C. III-V on silicon avalanche photodiodes by heteroepitaxy. *Opt. Lett.* **2019**, *44* (14), 3538−3541.

(16) Inoue, D.; Wan, Y.; Jung, D.; Norman, J.; Shang, C.; Nishiyama, N.; Arai, S.; Gossard, A.; Bowers, J. Low-dark current 10 Gbit/s operation of InAs/InGaAs quantum dot pin photodiode grown on on-axis (001) GaP/Si. *Appl. Phys. Lett.* **2018**, *113* (9), No. 093506.

(17) Sandall, I.; Ng, J. S.; David, J. P.; Tan, C. H.; Wang, T.; Liu, H. 1300 nm wavelength InAs quantum dot photodetector grown on silicon. *Opt. Express* **2012**, *20* (10), 10446−10452.

(18) Shang, C.; Wan, Y.; Norman, J. C.; Collins, N.; MacFarlane, I.; Dumont, M.; Liu, S.; Li, Q.; Lau, K. M.; Gossard, A. C.; et al. Low-Threshold Epitaxially Grown 1.3-μm InAs Quantum Dot Lasers on Patterned (001) Si. *IEEE J. Sel. Top. Quantum Electron.* **2019**, *25* (6), 1−7.

(19) Li, Q.; Wan, Y.; Liu, A. Y.; Gossard, A. C.; Bowers, J. E.; Hu, E. L.; Lau, K. M. 1.3-μm InAs quantum-dot micro-disk lasers on V-groove patterned and unpatterned (001) silicon. *Opt. Express* **2016**, *24* (18), 21038−21045.

(20) Huang, Z.; Li, C.; Liang, D.; Yu, K.; Santori, C.; Fiorentino, M.; Sorin, W.; Palermo, S.; Beausoleil, R. G. 25 Gbps low-voltage waveguide Si−Ge avalanche photodiode. *Optica* **2016**, *3* (8), 793−798.

(21) Chen, Y.; Xie, Z.; Huang, J.; Deng, Z.; Chen, B. High-speed uni-traveling carrier photodiode for 2 μm wavelength application. *Optica* **2019**, *6* (7), 884−889.

(22) Xie, Z.; Chen, Y.; Zhang, N.; Chen, B. InGaAsP/InP Uni-Traveling-Carrier Photodiode at 1064-nm Wavelength. *IEEE Photonics Technol. Lett.* **2019**, *31* (16), 1331−1334.

(23) Chen, Y.; Chai, X.; Xie, Z.; Deng, Z.; Zhang, N.; Zhou, Y.; Xu, Z.; Chen, J.; Chen, B. High-Speed Mid-Infrared Interband Cascade Photodetector Based on InAs/GaAsSb Type-II Superlattice. *J. Lightwave Technol.* **2019**, 1.

(24) Chen, Y.; Zhao, X.; Huang, J.; Deng, Z.; Cao, C.; Gong, Q.; Chen, B. Dynamic model and bandwidth characterization of InGaAs/GaAsSb type-II quantum wells PIN photodiodes. *Opt. Express* **2018**, *26* (26), 35034−35045.

(25) Duan, N.; Wang, S.; Ma, F.; Li, N.; Campbell, J. C.; Wang, C.; Coldren, L. A. High-speed and low-noise SACM avalanche photodiodes with an impact-ionization-engineered multiplication region. *IEEE Photonics Technol. Lett.* **2005**, *17* (8), 1719−1721.

(26) Ma, Y. J.; Zhang, Y. G.; Gu, Y.; Chen, X. Y.; Wang, P.; Juang, B. C.; Farrell, A.; Liang, B. L.; Huffaker, D. L.; Shi, Y. H.; et al. Enhanced Carrier Multiplication in InAs Quantum Dots for Bulk Avalanche Photodetector Applications. *Adv. Opt. Mater.* **2017**, *5* (9), 1601023.

https://dx.doi.org/10.1021/acsphotonics.9b01709
ACS Photonics 2020, 7, 528−533